Journal of Magnetism and Magnetic Materials 515 (2020) 167273

Contents lists available at ScienceDirect

Journal of Magnetism and Magnetic Materials

journal homepage: www.elsevier.com/locate/jmmm

Research articles

Effect of R substitution in spin glass $RFeTi_2O_7$ compounds

A. Arauzo[a,b,*], J. Bartolomé[a], J. Luzón[c], T. Drokina[d], G.A. Petrakovskii[d], M.S. Molokeev[d,e]

[a] Instituto de Nanociencia y Materiales de Aragón (INMA) and Departamento de Física de la Materia Condensada, CSIC- Universidad de Zaragoza, 50009 Zaragoza, Spain
[b] Servicio de Medidas Físicas, Universidad de Zaragoza, E-50009 Zaragoza, Spain
[c] Centro Universitario de la Defensa. Academia General Militar, Zaragoza, Spain
[d] Kirensky Institute of Physics, Federal Research Center KSC SB RAS, Akademgorodok, 50/38, Krasnoyarsk 660036, Russia
[e] Siberian Federal University, Krasnoyarsk 660041, Russia

ARTICLE INFO

Keywords:
Magnetism
Spin glass
Anisotropy
Frustration
Anisotropic exchange

ABSTRACT

Zirconolite oxides $R^{3+}Fe^{3+}Ti_2O_7$ (R rare earth element) are known to exhibit spin glass behaviour at low temperatures. Here we present a detailed study of these compounds for R = Eu, Gd, Dy, Ho, and Er, together with reviewed previous measurements on Sm, Tb, Tm, Yb and Lu, with the scope of determining the role played by the rare earth on their magnetic properties. They have been investigated using X-ray powder diffraction, and further characterized by magnetization, frequency dependent ac susceptibility and heat capacity measurements. $RFeTi_2O_7$ compounds are all isostructural showing orthorhombic structure, space group *Pcnb* at 300 K. Disorder of the magnetic ions in the $RFeTi_2O_7$ lattice induces spin glass behaviour at low temperatures, mainly due to the Fe sublattice. We show that magnetic rare earth ions participate in the spin glass state tuning its properties. The single ion anisotropy of the R^{3+} ions, excluding exchange interaction with other magnetic ions, has been calculated by *ab initio* methods, and expressed in terms of the *g* tensor of the ground doublet or quasi-doublet in Kramers (Sm, Dy, Er, Yb) and non-Kramers (Tb, Ho) ions, respectively, in an effective spin $S^* = 1/2$ model. In the case of R with a singlet ground state (Eu, Tm) or a multiplet state (Gd), the ion is isotropic. We show that the relative increase in the spin-glass temperature $\Delta T_{SG}^{R}/T_{SG}^{Fe}$ with respect to the $LuFeTi_2O_7$, where Lu is non-magnetic, correlates qualitatively with the product of the ratio g_z/g_J (R = Tb, Dy, Ho, and Er), or $g_\perp/g_J$ (R = Sm), times the ratio of exchange interactions $\tilde{J}_{R,Fe}/J_{Fe,Fe}$ determined from the paramagnetic room temperature susceptibility measurements. Besides, for increasing anisotropy the spin glass transition dynamics slows down to values typical of cluster glass. The coercive field below the transition is increased in the same trend. This paper explains the effect of the R-Fe exchange interaction and R single ion anisotropy on the spin-glass behaviour of these compounds.

1. Introduction

The physics of spin glass systems has been a field of scientific interest in the last decades [1–5]. There is a large variety of materials showing spin glass behaviour or exhibiting spin-glass-like features, being the current experimental and theoretical research on this field of great interest. The study of new spin-glass materials and their behaviour may reveal fascinating physical properties.

In canonical spin glasses, a 3d transition metal magnetic impurity is dissolved in a nonmagnetic noble metal host. In these systems the interaction between localized moments is mediated by conduction electrons through the long-range isotropic so-called RKKY interaction. Most of the anisotropy in canonical spin-glasses comes from the much weaker Dzyloshinskii-Moriya interaction. On the contrary, insulating spin glasses contain high concentration of magnetic ions presenting short range interactions which can be isotropic or anisotropic [5]. Antiferromagnetic (AFM) superexchange interactions are dominant in the magnetic oxide spin glasses, with the exception of Eu^{2+} containing oxides, where FM interactions are predominant [6,7]. The effect of single ion anisotropy has been addressed in a study of Fe phosphate glasses [8]. It was concluded that anisotropy tends to suppress fluctuations, giving rise to an increase of the freezing temperature.

Examples of insulating spin glasses containing either 3d metals or 4f rare earth ions are abundant [3,5]. Numerous are the studies of spin-glass phase in transition-metal oxides, in manganites [9–11], cobaltites [12], and cuprates [13,14], among others. Besides, spin glass behaviour is found in highly anisotropic 3d-metal heterometallic oxyborates like warwickites, which are naturally disordered materials [15]. Mixed crystals $Eu_xSr_{1-x}S$ with Eu^{2+} rare earth ion are well-known examples of Heisenberg spin glasses [16]. However the number of studies of spin

* Corresponding author.

https://doi.org/10.1016/j.jmmm.2020.167273
Received 31 March 2020; Received in revised form 16 June 2020; Accepted 29 July 2020
Available online 04 August 2020
0304-8853/

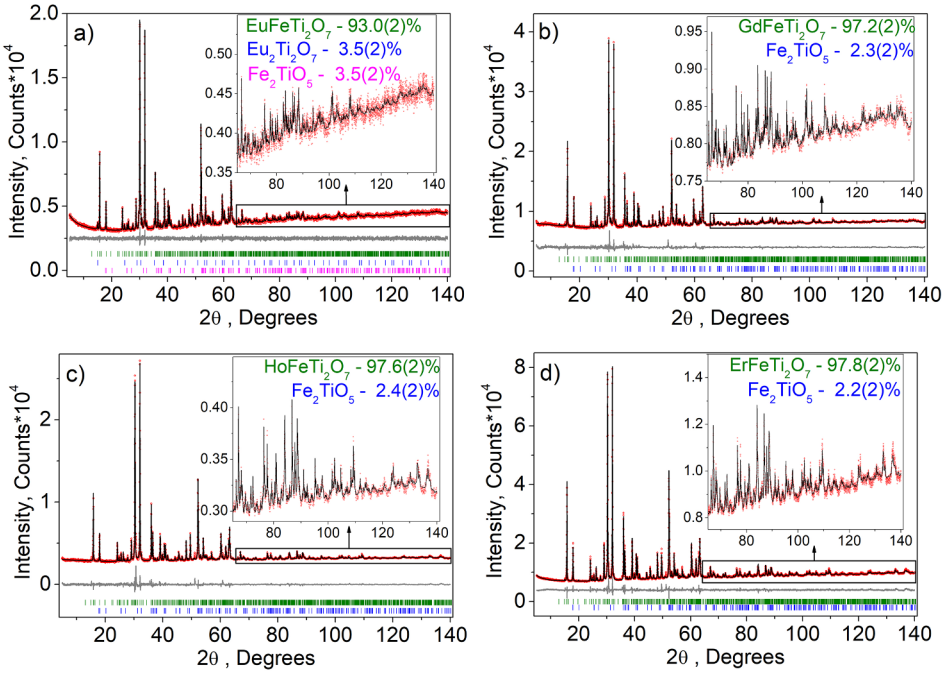

Fig. 1. Experimental (symbols), theoretical (line), and difference (lower line) X-ray diffraction patterns of the crystal structure of $RFeTi_2O_7$ samples collected at room temperature. a) $EuFeTi_2O_7$, b) $GdFeTi_2O_7$, c) $HoFeTi_2O_7$ and d) $ErFeTi_2O_7$. The substance under study contains a small percentage of the Fe_2TiO_5 impurity (see inset).

glasses containing both 3d and 4f ions is scarce [6]. The role of the presence of rare earth in spin glasses is important in binary metallic glasses [17], or in manganites [5,18]. The R = Pr and Nd doping induces structural modifications, and magnetic anisotropy gives rise to anisotropic spin glasses [19], since their atomic radius varies along the series, affecting the interatomic distances and hence, their magnetic phases. Besides, spin glass behavior has also been found in other aluminoborates containing Fe and R, where a dependence on the freezing temperature was observed depending on the Fe/R ratio [6].

Within this framework, rare-earth zirconolite oxides with general chemical formula $R^{3+}Fe^{3+}Ti_2O_7$ (R-rare earth element) can serve as model materials for the study of disordered systems and spin glass magnetism. These compounds conjugate the possibility of cation substitution with the presence of crystal lattice disorder together with competing magnetic interactions [20–24].

The $LuFeTi_2O_7$ compound serves as reference example, where Lu is non-magnetic, to show characteristic spin glass behaviour. Dc magnetic susceptibility measured in zero-field cooled (ZFC) and field-cooled (FC) conditions deviate from each other below the freezing temperature T_f = 4.5 K, ac susceptibility is frequency dependent, and heat capacity presents a rounded bump at that temperature range. Combining these results with X-ray diffraction and Mössbauer spectroscopy it was argued that the spin glass behavior stems from the disorder of the Fe atoms located at the different crystallographic positions [20,25].

The spin glass behaviour is maintained upon substitution of Lu by Sm [23], Gd [26], Tb [20], Dy [22], Tm [21], and Yb [24]. All of these compounds have similar magnetic spin glass behaviour, albeit dependent in detail on the rare-earth substitution. The purpose of this paper is to investigate the effect of the different magnetic rare earths on the spin glass behaviour of these series, depending on the R magnetic moment, and anisotropy. For this aim, besides the previously published results, we have carried out magnetic experiments and analysis of the new compounds with R = Eu, Er and Ho, and complemented the study on R = Gd and Dy. Within this study we analyse the role of rare earth ions, providing a plethora of anisotropy types, in the behaviour of insulating spin glasses combining transition metal and rare earth elements. The magnetization as a function of field, dc and ac susceptibilities, and heat capacity measurements have been performed to account for the effect of R substitution in the $RFeTi_2O_7$ compounds. *Ab initio* calculation of the R single ion anisotropy has been performed for each studied ion to aid in the analysis of the experimental results.

2. Experimental details

Powder samples of $RFeTi_2O_7$ (R = Eu, Gd, Ho and Er) were prepared by the solid state reaction method from a stoichiometric mixture of oxides Fe_2O_3, TiO_2, R_2O_3. The samples, formed in pellets, were subjected to a high-temperature treatment at 1250 °C. The chemical and phase compositions of the samples milled into powder were controlled by X-ray analysis. This synthesis method is identical to that employed in the preparation of all samples produced by the group in Krasnoyarsk (R = Sm, Tb, Dy, Tm, Yb and Lu), thus they can be safely compared.

The X-ray powder diffraction patterns of $RFeTi_2O_7$ samples for Rietveld analysis were collected on a Bruker D8-ADVANCE diffractometer (Cu-Kα radiation) with linear VANTEC detector at room temperature. All refinements of the patterns were performed with TOPAS 4.2 (Bruker).

Polycrystalline $RFeTi_2O_7$ magnetization measurements were carried out with a superconducting quantum-interference device (SQUID) magnetometer in the temperature range of 2–300 K and external magnetic field of 500 Oe. The magnetization as a function of temperature was measured both in zero-field-cooled (ZFC) and field-cooled (FC) regimes.

Ac susceptibility measurements were performed in a SQUID magnetometer, in the frequency range $0.01 < f < 1400$ Hz, with an exciting field of 4 Oe.

Heat capacity as a function of temperature was measured on pellets using a Quantum Design PPMS (Physical Properties Measurement System) in the temperature range 1.9–300 K. The sample was fixed to the sample holder with Apiezon grease.

3. Results and discussion

3.1. Structure of $RFeTi_2O_7$

The structures of the synthesized $RFeTi_2O_7$ (R = Eu, Gd, Ho and Er) crystals have been determined from data of an X-ray diffraction experiment performed for a powder sample. The previously X-ray studied $GdGaTi_2O_7$ [27] was taken as the initial model for the determination of the crystal structure and atomic positions. The X-ray diffraction pattern of the crystal structure of $RFeTi_2O_7$ collected at room-temperature is shown in Fig. 1 for R = Eu, Gd, Ho and Er. Diffraction pattern for R = Dy has been published in a previous structural study of $DyFeTi_2O_7$ [22]. Crystallographic data for $DyFeTi_2O_7$ can be found in the Crystallography Open Database with No. COD-1529335.

According to X-ray diffraction data the prepared compounds crystallize in the orthorhombic crystal structure, with space group *Pcnb*, at room temperature. All compounds are isostructural to Zirconolite structure, $CaZrTi_2O_7$ [26]. Note that a small amount of the impurity Fe_2TiO_5 (2–4%) was found in the substances. We have checked that this second phase does not affect our conclusions, since its magnetic contribution is orders of magnitude smaller than that of $RFeTi_2O_7$ (see Fig. S3). The key structural parameters of the compounds $RFeTi_2O_7$ (R = Eu, Gd, Ho and Er) and X-ray experimental details are given in Table 1. Atomic coordinates and thermal parameters are presented in Table SI. The schematic crystal structure of $RFeTi_2O_7$ compound is shown in Fig. 2a.

Occupation probability *p* of all ions after refinement is presented in Table SI. The unit cell of $RFeTi_2O_7$ is constructed by four-vertex, five-vertex, six-vertex, and eight-vertex oxygen polyhedra; the rare earth cation is arranged in the eight-vertex polyhedron (see Figs. 2 and 3). There are five nonequivalent iron sites: the two iron positions in the oxygen octahedron consisting of the Fe_t tetrahedron and Fe_f (Fe′, Fe″) five-vertex polyhedron, and the three positions ((Ti1/Fe1), (Ti2/Fe2), and (Ti3/Fe3)) in the mixed octahedral (see Fig. 2a and b). The populations of the mixed Ti-Fe sites are different (Table SI). The tetrahedral sites are populated with Fe. These Fe atoms may be located out of the tetrahedra and populate neighboring sites Fe′ and Fe″ with coordination of five (Fig. 2). Thus the peculiarities of the titanate structure indicate a disorder of the magnetic iron ions distribution mainly over five structural sites in $RFeTi_2O_7$ compound.

Table 1
$RFeTi_2O_7$. Crystallographic parameters at T = 300 K.

Complex	$EuFeTi_2O_7$	$GdFeTi_2O_7$	$HoFeTi_2O_7$	$ErFeTi_2O_7$
CCDC	190,039	190,038	190,040	1,900,752
Space group *Pcnb*				
a, Å	9.8356(2)	9.8321(2)	9.8353(2)	9.8285(1)
b, Å	13.6708(2)	13.6498(2)	13.5572(2)	13.5428(2)
c, Å	7.4491(1)	7.4250(1)	7.3497(1)	7.3378(1)
V, Å^3	1001.61(3)	996.49(3)	980.01(3)	976.70(2)
Z	8	8	8	8
D_x, g/cm^3	5.533	5.639	5.796	5.860
μ, mm^{-1}	137.302	136.645	78.909	80.795
Radiation	Cu-Kα	Cu-Kα	Cu-Kα	Cu-Kα
2θ-range, deg.	5–140	5–140	5–140	5–140
Number of reflections	958	944	939	933
Number of refined parameters	82	84	82	73
R_{wp}, %	1.72	1.128	1.187	2.40
R_{exp}, %	1.58	0.577	0.915	1.04
R_p, %	1.36	0.995	1.657	1.59
GOF (χ)	1.09	1.956	2.063	2.31
R_{Bragg}, %	0.29	0.424	0.780	0.87

Note: *V* is the unit cell volume, *Z* is the number of formula units in the cell, D_x is the calculated density, μ is the absorption coefficient, R_{wp} is the weight profile uncertainly factor, R_{exp} is the expected uncertainly factor, R_p is the profile uncertainly factor, *GOF* (χ) is the adjustment quality, and R_{Bragg} is the Bragg integral discrepancy factor.

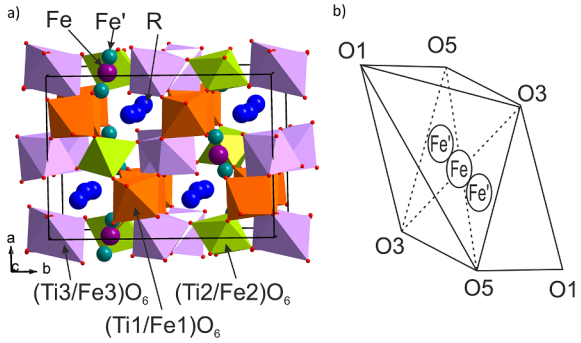

Fig. 2. $RFeTi_2O_7$. a) The schematic crystal structure (left) and b) its fragment (right).

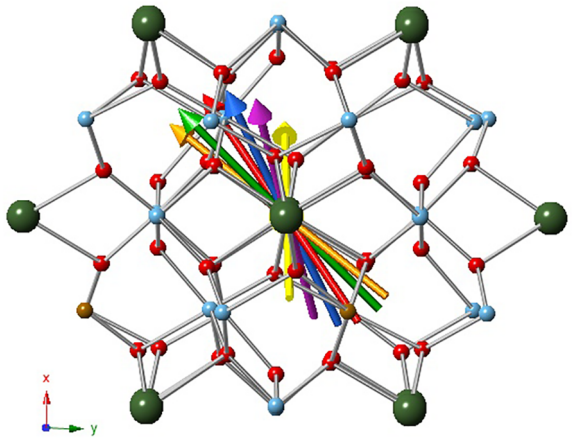

Fig. 3. Easy magnetization vectors of the ground state as calculated by ab initio method. Color code (Tb: red, Dy: orange, Ho: yellow, Er: green, Tm: blue, Yb: violet). View along z axis of the crystal. (For interpretation of the references to color in this figure legend, the reader is referred to the web version of this article.)

The rare earth cation substitution does not change the crystal structure symmetry. The availability of the different non-equivalent positions for the magnetic Fe^{3+} ions in the unit cell induces structural disorder. Crystallographic data (excluding structure factors) for the structural analysis have been deposited with the Cambridge Crystallographic Data Centre, Nos CCDC-190038 ($GdFeTi_2O_7$), CCDC-190039 ($EuFeTi_2O_7$), CCDC- 1,900,752 ($ErFeTi_2O_7$) and CCDC-190040 ($HoFeTi_2O_7$).

3.2. Ab initio calculations of the ground state.

The magnetic anisotropy of the ground state of the rare-earth ions in the series has been investigated by *ab initio* calculations using the relativistic quantum chemistry method RASSI-SO [28] as implemented in the MOLCAS quantum chemistry package [29]. Each molecular cluster used in the calculations included the studied rare-earth ion and the four closest atom shells (oxygen-3d/4f ion-oxygen-3d/4f ion) (see Fig. 3), where the Fe ions have been replaced by Ga(III) ions and the neighbor rare-earth ions by La(III) ions in order to have closed-shell ions. Additionally, the clusters were embedded in a distribution of punctual charges fitting the Madelung's potential produced by the rest of the crystal inside the cluster region. The atomic positions for the cluster models were extracted from the X-ray crystal structures where, for the sites with a Fe/Ti occupational disorder, only the most probable ion was considered. All the atoms were represented by basis sets of atomic natural orbitals from the ANO RCC library [30]. The following contractions were used: [9s8p6d4f2g1h] for the R ion, [4s3p1d] for the O atoms in the first shell around the R ion, triple quality basis sets for the

Table 2
Ab initio calculated values for the g tensor components of the ground state, and energy to the first and second excited states, for the different R^{3+} ions in $RFeTi_2O_7$ compounds.

	g_x	g_y	g_z	E_0 (K)	E_1 (K)
Sm	0.49	0.46	0.06		302
Eu	singlet				
Gd	2	2	2		
Tb	0	0	15.25	2.18	36
Dy	0.03	0.02	19.56		139
Ho	0	0	19.53	0.73	61
Er	2.04	3.15	12.93		76
Tm	singlet				78
Yb	1.63	2.90	5.6		463

ions in the second shell and double quality basis sets for the rest of the atoms. Finally, the chosen CASSCF active space consisted of the R 4f orbitals.

The computed single ion ground state anisotropy has been expressed in terms of the *g* tensor components for the ground doublet in the Kramers ions Sm, Dy, Er and Yb, and for the pseudo-doublet in non-Kramers Tb and Ho, in a $S^* = 1/2$ effective spin formulation. Tm has a singlet ground state, thus the *g* tensor description is not applicable. The resulting *g* tensor values, the energy gap inside the pseudo-doublet for the non-Kramers ions (E_0) and the energy gap between the ground doublet state and the next lowest state (E_1) for all the ions are collected in Table 2. Table 2 is completed with the Eu and Gd ions, which were not computed since the ground state of the first one is a singlet ($J = 0$) and the second one has not magnetic anisotropy ($L = 0$).

Thus, the ground state for Gd is isotropic, for Tb, Dy Ho and Er the anisotropy is strongly uniaxial, Yb is also uniaxial but less anisotropic, in Sm it is planar, and Eu and Tm have a singlet ground state, supporting no magnetic moment. The calculated easy axis of magnetization lies in different directions respect to crystallographic axes for the different rare-earth element (see Fig. 3 and Fig. S1, Fig. S2 of ESI). No apparent correlation is observed unless a tendency for all the magnetization vectors to lie opposite to (1 1 0) crystal axis.

3.3. Magnetic properties

3.3.1. Dc magnetic susceptibility

The temperature dependence of the magnetic susceptibility in an external magnetic field of 0.5 kOe has been measured for $RFeTi_2O_7$ (R = Eu, Gd, Dy, Ho and Er). The inverse magnetic susceptibility $1/\chi$ has been fitted to a Curie-Weiss law in the $150 \leq T \leq 300$ K range. Obtained parameters are included in Table 3. All the studied compounds show negative Neel asymptotic behaviour, indicating that the dominant interaction is antiferromagnetic. In Fig. 4 the $C/\chi = T - \theta_W$ temperature dependence is depicted for every compound, where *C* is the obtained Curie-Weiss constant obtained in the fit (see Table 3). For the sake of comparison, data for R = Tb and Lu, measured and published in a previous study by our group [20], have been used in the analysis.

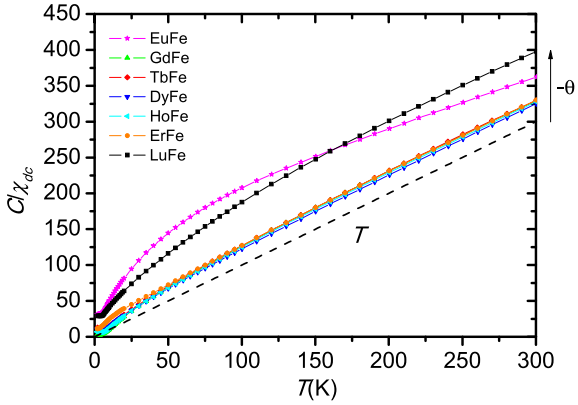

Fig. 4. Temperature dependence of the inverse magnetic susceptibility of $RFeTi_2O_7$ (denoted 'RFe' in legend) multiplied by the obtained Curie-Weiss constant *C* for each rare-earth substitution ($H = 0.5$ kOe). The dashed line represents a Curie-Weiss temperature dependence defined by $C/\chi = T - \theta_W$ (for Neel asymptotic temperature $\theta_W = 0$ K).

It is clearly observed that all the rare earth compounds, except for R = Eu, follow a *T* slope at high temperature. The reason for the discrepancy in the case of Eu is that we have not considered a temperature independent contribution to the susceptibility which is large in the case of Eu^{3+} ion, due to the low lying excited states [31]. The experimentally determined effective magnetic moment for all the materials is given in Table 3. These values of the effective moment contain the contribution from the rare earth ion and the Fe^{3+} ion, which we can consider as additive in the high temperature range ($T > 150$ K). The value of the effective moment $\mu_{Fe} = 5.16 \pm 0.06\ \mu_B$ for the Fe sublattice in the $LuFeTi_2O_7$ compound (Lu non-magnetic) may be used to determine the values of the experimental effective moment μ_R for the other R substitutions through the expression $\mu_R = (\mu_{eff}^2 - \mu_{Fe}^2)^{1/2} = m_R\mu_B$.The experimental values obtained agree excellently with the expected values for free *R*, according to Hunds rule $\mu_R = g_J[J(J+1)]^{1/2}\mu_B$, where g_J is the Lande factor for R (see Fig. S4 of ESI).

The above agreement is rather good for most of the rare earth ions. Let us remember that we are analyzing the macroscopic magnetic susceptibility of polycrystalline samples at high temperatures. In fact, the crystal field interaction which generally splits the ground state *J*

Table 3
Obtained parameters for the fit of the $\chi^{-1}(T)$ experimental values to a Curie-Weiss law, *C* and θ_W. Calculated effective moment of the different compounds, μ_{eff}, and rare-earth effective moment, μ_R in μ_B units. High temperature Weiss interaction parameter θ_{RFe} calculated for the different rare-earths studied in this work. Values for Sm, Tm and Yb have been obtained from references [21,23,24], respectively. Mean exchange constants of the magnetic interaction between R and Fe are given in units of k_B.

R	*C* (emuK/mol)	θ_w (K)	μ_{eff} (μ_B)	μ_R (μ_B)	θ_{RFe} (K)	$\bar{J}_{R,Fe}/k_B$ (K)
Sm [23]	3.7	−95	5.55	2.04	−12.5	−0.68
Eu	4.7 ± 0.4	−134 ± 14	6.2 ± 0.2	3.4 ± 0.5		
Gd	10.8 ± 0.1	−30 ± 3	9.28 ± 0.04	7.71 ± 0.09	0.6 ± 2.8-	0.06 ± 0.07
Tb[a]	14.9 ± 0.1	−31 ± 2	10.93 ± 0.05	9.63 ± 0.10	−10.4 ± 3.0	−0.63 ± 0.05
Dy	17.0 ± 0.1	−25 ± 1	11.68 ± 0.02	10.48 ± 0.05	−7.3 ± 1.4	−0.36 ± 0.02
Ho	17.0 ± 0.1	−28 ± 1	11.68 ± 0.04	10.47 ± 0.09	−11.0 ± 1.5	−0.51 ± 0.02
Er	14.8 ± 0.1	−30 ± 2	10.87 ± 0.04	9.56 ± 0.08	−9.4 ± 2.5	−0.46 ± 0.03
Tm [21]	10.4	−43	9.11	7.51	−11.7	−0.71
Yb [24]	7.0	−127	7.48	5.41	−79.5	−6.51
Lu[a]	3.3 ± 0.1	−100 ± 8	5.16 ± 0.06	0.00		

[a] Values derived from experimental data from previous study [20]. Previously reported values for Sm, Tm and Yb have been also included.

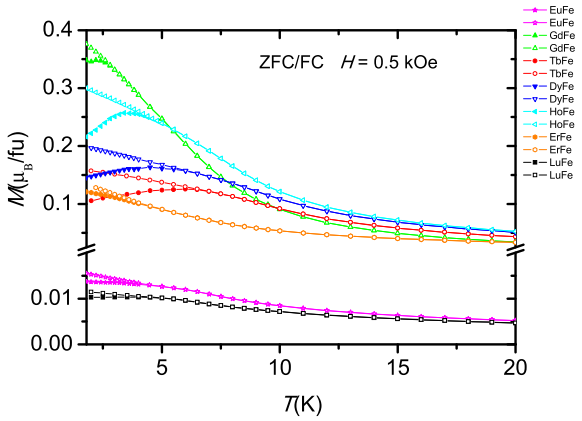

Fig. 5. Temperature dependence of the magnetization $M(T)$ (ZFC (solid symbols) and FC (open symbols) curves at an external magnetic field $H = 0.5$ kOe in $RFeTi_2O_7$ (R = Eu, Gd, Dy, Ho and Er) together with $TbFeTi_2O_7$ and $LuFeTi_2O_7$ results [20].

multiplets, determining the collective temperature behavior mainly at low temperatures, is not considered at the present stage of analysis. In our naïve approach we estimate the overall average contribution at temperatures near room temperature considering that all the CF split levels are populated. The obtained estimation of the effective interaction given by Neel asymptotic temperature θ_W may differ from the interaction determined at low temperature, which is anisotropic for some R substitutions.

As temperature decreases, the $\chi(T)$ behavior strongly deviates from a Curie-Weiss law, due to depopulation of crystal field split levels and magnetic interaction effects. There are no previous studies of R^{3+} single ion anisotropy in $RFeTi_2O_7$ compounds.

Magnetization measurements as a function of temperature both in zero-field-cooled (ZFC) and field-cooled (FC) regimes for external magnetic field $H = 0.5$ kOe show a bifurcation at low temperatures for all measured compounds, which is a revealing characteristic for spin glasses at the freezing temperature T_f (see Fig. 5). Similar behaviour in $M(T)$ at $H = 0.5$ kOe has been observed for Sm [23], Tm [21], and Yb [24]. ZFC/FC curves of $RFeTi_2O_7$ for magnetic R cannot be explained in terms of a superposition of the spin glass behavior of the Fe^{3+} sublattice and a paramagnetic behavior of the R^{3+}. The large deviation observed between ZFC and FC curves as compared to $LuFeTi_2O_7$ clearly indicates that rare earth magnetic sublattice is magnetically coupled to the iron sublattice. Even for the $ErFeTi_2O_7$ where no maximum is observed, the splitting of the curves is one order of magnitude larger than for Lu substitution. The so obtained freezing temperature, defined as the temperature below which irreversibility is observed, depends on the rare earth ion, varying from 2.6 K for $GdFeTi_2O_7$ to 6.5 K for $TbFeTi_2O_7$. Additionally, the degree of irreversibility (relative divergence between ZFC and FC curves), is strongly R-dependent, being larger for the R = Tb, Dy and Ho substitutions as compared with that in the Er, Lu, Gd, (see Fig. 5). The reason for this behavior stems from the larger anisotropy induced by the presence of the R in the former cases, while the anisotropy is lower for the Er, and Gd is isotropic. The magnetism for Eu and Lu stems from the Fe sublattice. We confirm this statement below.

3.3.2. Magnetic field dependence of the low temperature magnetization

The magnetization hysteresis curves $M(H)$ at $T = 2.0$ K have been measured at -50 kOe $< H <$ 50 kOe. The $LuFeTi_2O_7$ has an antiferromagnetic behavior evidenced by the slope at the highest field, and a coercive field of $H_c = 143$ Oe. The presence of the magnetic R sublattice gives rise to an increase in the $M(H)$ value and an increase in the coercive field with the trend Er < Ho < Dy < Tb (see Fig. 6 inset). Although the highest value of $M(H)$ is achieved by the $GdFeTi_2O_7$, it has

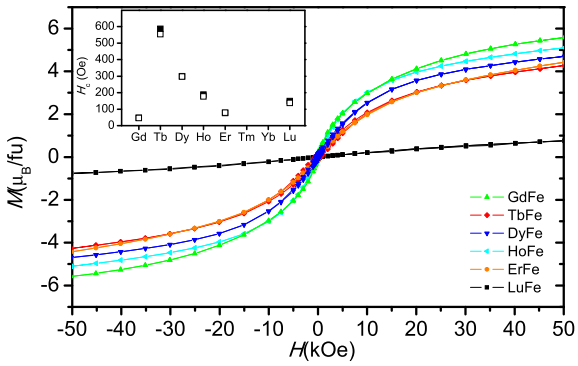

Fig. 6. Hysteresis loop at 2.0 K up to 50 kOe for R = Gd, Tb. Dy, Ho, Er and Lu. Inset: Coercive field values, H_c (bold squares), $-H_c$ (open squares).

the lowest H_c of the series, even lower than the Lu compound. The exceptional behavior of the Gd substitution can be related to the very small Fe-Gd exchange interaction and its isotropic character, leading as a consequence to the magnetic softening of the $GdFeTi_2O_7$ compound. The highest coercivity is found for the Tb substitution, although its anisotropy is not the highest, as estimated in the ab initio calculations. We shall return to this point later.

3.3.3. Ac susceptibility measurements

We have carried out a study of the dynamical properties of the spin glass transition by means of ac susceptibility. Moreover, this technique allows us determining the freezing temperature at very low magnetic field, given the spin-glass state sensitivity to magnetic field. The results of ac susceptibility measurements at different excitation frequencies f and fixed driving field amplitude of 4 Oe on the powder sample $HoFeTi_2O_7$ are shown in Fig. 7a and b. Very similar results are obtained for the other substitutions (see ESI S4). The onset of the spin glass transition is defined by a cusp in the in-phase susceptibility $\chi'(T)$ or by an inflection point in the out-of-phase component, $\chi''(T)$. We observe that in the whole series, except for the $LuFeTi_2O_7$ compound, the cusp in the $\chi'(T)$ is smeared out as frequency increases, therefore we have taken the well resolved maximum slope in $\chi''(T)$ as the $T_f(f)$ onset. The freezing temperature varies with frequency, for instance, for $HoFeTi_2O_7$, freezing temperature increases from the lowest value $T_f \sim 6.7$ K at 0.1 Hz, to $T_f \sim 7.6$ K at the highest frequency measured, 1400 Hz (see Fig. 7b).

A way to evaluate the frequency sensitivity of freezing temperature is to calculate the p_f factor, defined as the relative shift in freezing temperature per decade of frequency, $p_f = \Delta T_f/[T_f\, \Delta(\log f)]$. Obtained values are given in Table 4. It is observed that values for R = Lu, and Gd are rather low and within the range of values obtained in canonical spin-glasses: 0.005–0.018 [2]. However, for Dy, Ho and Tb, the variation of T_f with frequency is larger, with p_f values of about 0.03 (see ESI, S5). Observed differences deserve a deeper analysis.

The values of $T_f(\omega)$ for the different R substitutions are depicted in Fig. 7c, and have been analysed within the Dynamical scaling theory near a phase transition at T_c. According to this theory, the relaxation time follows the critical slowing down law, which in terms of frequency predicts $f = f_0(T_f(\omega)/T_c - 1)^{z\nu}$, where $T_f(\omega)$ is the frequency dependent freezing temperature determined by the inflexion point in χ''(T) and T_c is the phase transition temperature in the limit of zero frequency, f_0 is the characteristic frequency constant, ν is the critical exponent for the correlation length ξ and z is the dynamical exponent. The obtained fit parameters are collected in Table 4, together with those for the Lu and Tb substitutions. We note that the critical behaviour of the different R provides a whole panoply of results. Isotropic Gd shows very similar results to Lu, with high values for f_0, indicating a fast relaxation process, typical of canonical spin-glasses [2]. On the other hand, Ising ions like Tb, Dy, Ho, and Er have a much lower f_0 parameter, which is

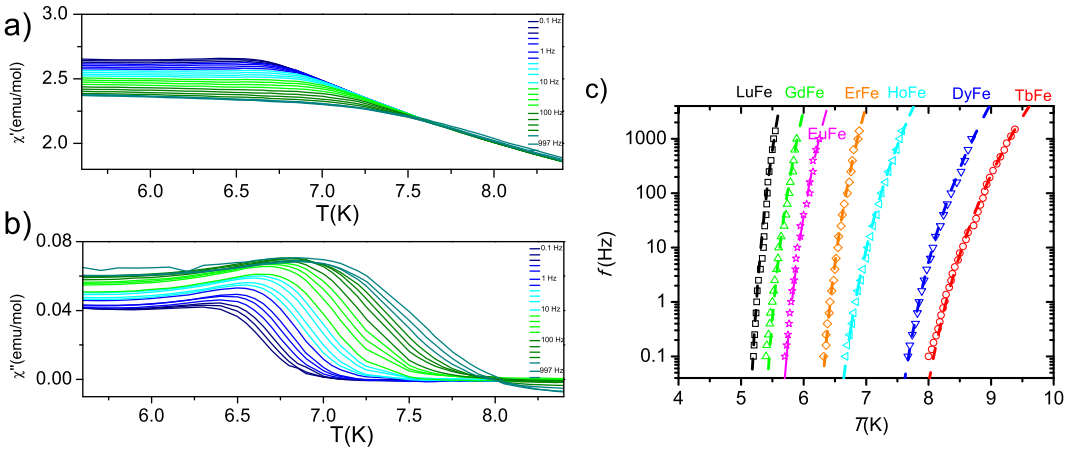

Fig. 7. a) $HoFeTi_2O_7$. Temperature dependences of the in-phase component χ' and b) the out-of-phase component χ'' of ac magnetic susceptibilities using an ac magnetic field of 4 Oe as a function of frequency. c) Variation of the spin-glass transition temperature as a function of frequency for $RFeTi_2O_7$ (R = Eu, Gd, Dy, Ho and Er) compared to $TbFeTi_2O_7$ and $LuFeTi_2O_7$ results [20]. Dashed lines show the fit to a critical slowing down law.

characteristic of slower relaxation similar to values observed in cluster spin glasses [2,32–35]. Obtained values for T_c are very close, slightly lower, than the experimental value of T_f at the lowest frequency, taken as T_{SG} (column 3 in Table 4), in excellent agreement to what it would be expected for the zero frequency transition temperature.

The slower relaxation obtained for the strongly anisotropic ions, Tb, Dy, Ho an Er, means that the time constant for a spin flip is reduced by the anisotropic interaction. This behaviour, which is typical of clustering in spin glasses, would indicate a stronger interaction between the rare earth and the iron for the more anisotropic ions.

In the following analysis and discussion, we will take as spin-glass transition temperatures, T_{SG}, those obtained by ac magnetic susceptibility at the lowest frequency, 0.1 Hz (Table 4, column 3), thus minimizing variations with applied magnetic field and frequency. For the sake of comparison we have taken obtained values from previous studies, $T_f = T_{SG}^{Sm} = 7$K for R = Sm [23], $T_f = T_{SG}^{Tm} = 6$K for R = Tm [21] and $T_f = T_{SG}^{Yb} = 5.2$K for R = Yb [24].

From the dynamical analysis of the freezing temperature we observe a clear dependence of the transition temperature and their dynamics with the anisotropy of the R ion. The same trend observed in H_c is repeated for the spin glass temperature, increasing in the series Er < Ho < Dy < Tb. The obtained characteristic spin flip relaxation time, $\tau_0 = 2\pi/f_0$, as well, is following the same trend, demonstrating how the rare-earth ion anisotropy is influencing the spin glass state in these materials.

3.4. Calorimetric properties

Heat capacity measurements as a function of temperature were performed on the $RFeTi_2O_7$ series. Data are shown in Fig. 8. They show no peak associated with a long range magnetic ordering transition, instead there appears a very broad contribution with a maximum at about 5–10 K which can be ascribed to the spin-glass state. At low temperature a linear dependence with temperature is observed, typical of spin glasses, related to the intrinsic spin disorder. The data have been extrapolated to very low temperatures (T < 2 K) following the experimentally obtained T slope.

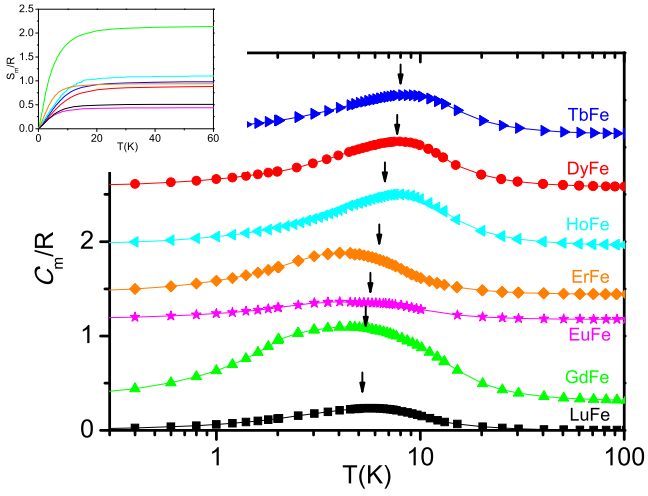

Fig. 8. Temperature dependence of the magnetic contribution to the heat capacity, C_m, of $RFeTi_2O_7$, (R = Eu, Gd, Tb, Dy, Ho, Er and Lu) in a stacked plot. Arrows indicate the T_{SG} value for each compound. Values below 2 K have been obtained by data extrapolation considering a linear T dependence. Inset: Calculated associated magnetic entropy, S_m.

For $GdFeTi_2O_7$ the associated magnetic entropy has been found to increase up to a maximum value of about 2.13 R at 50 K (see Inset Fig. 8). This value is much lower than the molar entropy expected for a $S = 5/2$ Fe^{3+} ion and a $S = 7/2$ Gd^{3+} ion per formula unit, which is an

Table 4
Spin-glass transition temperature determined by dc at H = 0.5 kOe and ac susceptibility experiments (0.1 Hz, 4 Oe). Best fit parameters for the frequency dependence of the spin-glass transition.

	T_f (K)500 Oe	T_{SG} (K)*ac*	p_f	T_c (K)	f_o (Hz)	$z\nu$
EuFe	4.5 ± 0.2	5.7 ± 0.1	0.022	5.4 ± 0.5	3 ± 1·10^{10}	9 ± 1
GdFe	2.6 ± 0.2	5.4 ± 0.1	0.017	5.2 ± 0.5	7.0 ± 0.3·10^{10}	9 ± 1
TbFe	6.5 ± 0.5	8.0 ± 0.1	0.034	7.4 ± 0.5	2.1 ± 0.1 10^{8}	9 ± 1
DyFe	6.0 ± 0.5	7.7 ± 0.1	0.029	7.1 ± 0.5	6.4 ± 0.2·10^{8}	9 ± 1
HoFe	5.0 ± 0.5	6.7 ± 0.1	0.029	6.2 ± 0.1	1.0 ± 0.5·10^{9}	9 ± 1
ErFe	5.0 ± 0.5	6.3 ± 0.1	0.020	6.0 ± 0.5	7 ± 4·10^{10}	9 ± 1
LuFe	4.5 ± 0.2	5.2 ± 0.1	0.014	5.0 ± 0.5	6 ± 4·10^{11}	9 ± 1

indication of the multiplicity of the ground state typical of spin-glasses. It is remarkable the large increase of entropy in the Gd case, evidently ascribable to the larger Gd spin and its isotropic character.

A similar analysis can be made for the rest of compounds: in all cases the calculated entropy yields much smaller values than those expected for a regular magnetic ordering transition, evidencing extensive ground state entropy.

Typically, magnetic specific heat in spin glasses shows a broad maximum centred at 20–40 percent above the transition [3], which agrees with observed contribution for the different complexes.

4. Discussion

The experimental results shown above reveal the important role played by rare earth on the spin-glass characteristics of these compounds. In this section we want to discuss and rationalize these observations by means of a comprehensive analysis of the effect played by the Heisenberg and non-Heisenberg exchange interaction in these spin-glass compounds. Temperature plays an important role in the crossover from isotropic behaviour at high temperatures to anisotropic at low temperatures in some compounds (Sm, Dy, Ho, Er, Tm), since the anisotropic *g* tensor of the rare earth ions in the crystal field split ground state of the R ion conditions the character of the interaction Hamiltonian, as we show below.

4.1. High temperature

The two sublattice magnetic system in an applied field H can be modeled by the Hamiltonian:

$$\mathscr{H} = \mathscr{H}_{Fe} + \mathscr{H}_{R,Fe} + \mathscr{H}_{R} + \mathscr{H}_{Z} \tag{1}$$

where

$$\mathscr{H}_{Fe} = -\sum_{i>j}^{Fe} 2J_{Fe,i,Fe,j}\vec{S}_{Fe,i}\bullet\vec{S}_{Fe,j} \tag{2}$$

corresponds to the Fe-Fe exchange interaction, and $S_{\mathrm{Fe}} = 2$ for all Fe atoms, $\mathscr{H}_{R}$ to the R-R interaction that we consider negligible in the present case, and $\mathscr{H}_{R,Fe}$ to the Fe spin $\vec{S}_{Fe}$–R spin$\vec{S}_{R}$ exchange interaction, where the sum is extended to the nearest neighbors. In this case $J_{R,i,Fe,j}$ may depend on the R orbital moment, and it has been argued that when exchange is mediated by oxygen atoms, the d-f interaction consists of two components: an isotropic Heisenberg, and a non-Heisenberg anisotropic component, with both components competing when they are of opposite signs.[36] However, at high temperatures it has been proven in Section 3.3 that the rare earth is well described by the total angular momentum wavefunctions $|J,M\rangle$ of R, and consequently the isotropic exchange interaction is adequate to describe the high temperature magnetic paramagnetic behavior.

$$\mathscr{H}_{R,Fe} = -2\sum_{i>j}^{Fe,R} J_{R,i,Fe,j}\vec{S}_{Fe,i}\bullet\vec{S}_{R,j} \tag{3}$$

It may be expressed in terms of the J_{R} angular momentum applying the relation between $\vec{S}_{R}$ and $\vec{J}_{R}$ angular momentum operators for R. $\vec{S}_{R} = (g_J - 1)\vec{J}_{R}$, One obtains:

$$\mathscr{H}_{R,Fe} = -2\sum_{i>j}^{Fe,R} \tilde{J}_{R,Fe,i,j}\vec{S}_{i}\bullet\vec{J}_{j} \tag{4}$$

where $\tilde{J}_{R,Fe} = (g_J - 1)J_{R,Fe}$. For the sake of notation simplification, $\vec{S}$ is the Fe spin, $\vec{J}$ is the R angular momentum, and $\tilde{J}_{R,Fe}$ corresponds to the exchange interaction between them.

The Weiss constants θ_W obtained from magnetic susceptibility measurements are collected in Table 3. For the $LuFeTi_2O_7$ the Weiss constant for the Fe sublattice is obtained and denoted as θ_{Fe}. Since they are determined from a high temperature range where the paramagnetic fluctuations are dominant, they may be used to evaluate the average Fe-Fe and Fe-R interactions.

A mean field method for two different magnetic sublattices has been applied, following the method proposed in [6]. Assuming that at high temperature each R and Fe sublattice follows a Curie-Weiss law in absence of the Fe and R sublattices, respectively, $\chi_A(T) = \frac{C_A}{T-\theta_A}$, where C_{A} and θ_{A} are the Curie and Weiss constant, respectively, for ion A, and $\chi_{RFe}(T) = \frac{C_{Fe}+C_R}{T-\theta_W}$ for the two sublattice system, with $C_{Fe} = \frac{Nm_{Fe}^2\mu_B^2}{3k_B}$, and $C_R = \frac{Nm_R^2\mu_B^2}{3k_B}$ The following relation between the Weiss constants of the two sublattices is obtained:

$$\theta_W = \frac{C_{Fe}\theta_{Fe} + C_R\theta_R + 2(C_{Fe}C_R)^{1/2}\theta_{RFe}}{C_{Fe}+C_R} \tag{5}$$

Assuming that the R-R 4f-4f interaction is much weaker than between R-Fe, 4f-3d and Fe-Fe 3d-3d interactions, as can be expected from the internal orbital of the R 4f electrons, the parameter θ_{RFe}can be extracted from the experimental data in Table 3:

$$\theta_{\mathrm{RFe}} = \frac{(\mu_{Fe}^2 + \mu_R^2)\theta_W - \mu_{Fe}^2\theta_{Fe}}{2\mu_{Fe}\mu_R} \tag{6}$$

The results are given in Table 3. The average exchange interactions may be estimated within a next nearest neighbor scheme if the number of neighbors B to each atom A, $Z_{A,B}$, is known, as is the present case, if one takes account of the five types of sites, where Fe can be placed and their respective statistical weights (see S6, ESI). One obtains for $Z_{\mathrm{Fe,Fe}} = 2.9$, the value

$$\frac{J_{FeFe}}{k_B} = \frac{6\theta_{Fe}}{\mu_{Fe}^2 Z_{Fe,Fe}} = -7.8\mathrm{K} \tag{7}$$

A similar expression is obtained for the average $\tilde{J}_{R,Fe}$interaction constant:

$$\frac{\tilde{J}_{R,Fe}}{k_B} = \frac{12\theta_{RFe}\bullet g_J}{\mu_R\mu_{Fe}(Z_{R,Fe} + Z_{Fe,R})} \tag{8}$$

In this case, we distinguish between the average number of Fe atoms around R ion, $Z_{\mathrm{R,Fe}} = 2.5$ from R atoms around Fe, $Z_{\mathrm{Fe,R}} = 3.5$ (see S6, ESI). The exchange constants $\tilde{J}_{R,Fe}$ are collected in Table 3. The positive value for Gd implies that this interaction is ferromagnetic (FM), while all the rest are antiferromagnetic (AFM), and are more than one order of magnitude weaker than the J_{FeFe} interaction. Thus, it can be expected that the Fe sublattice and its internal FeFe interaction are dominant in establishing the magnetic behavior of these systems, albeit, modulated by the presence of the R moments weakly coupled to the former.

The values of θ_{RFe} oscillate along the heavy element series around the value −10 K, which means that the average R-Fe interaction is very similar in all cases, except Gd and Yb. We note that in the case of Gd^{3+} the value of θ_{RFe} is approximately zero, within the error bar, which implies that this interaction is practically negligible. On the other hand, it is also remarkable the very large value obtained for θ_{RFe} for R = Yb. This value is calculated with Eq. (6), taking as $\theta_{\mathrm{W}} = -127$ K experimentally determined from the $\chi^{-1}(T)$ fit in reference [24]. Such a high value for the asymptotic Neel temperature may be originated in the large crystal field splitting usually observed for Yb^{3+} as compared with the rest of studied magnetic R^{3+}. Yb^{3+} ground state is a doublet with the first excited state lying at an energy of > 460 K above Ground State in $YbFeTi_2O_7$. Therefore, the Curie-Weiss law is not obeyed in the experimental temperature domain measured. Fit of the experimental $\chi(T)$ using the Crystal Field levels obtained by Inelastic Neutron Scattering in $Ba_3Yb_2Zn_5O_{11}$ yields an AF molecular field constant, $\lambda = -9$ mol/emu. That result is equivalent to an approximate value of $\theta_{\mathrm{W}} = \lambda C = -23$ K, in the Curie-Weiss formulation, whereas the high temperature asymptotic determination would yield a much larger value for θ_{W}. This would explain the discrepancy observed in the calculated $\tilde{J}_{R,Fe}/k_B$ for Yb (see Table 3).

4.2. Low temperature

The ratio $|\theta_W|/T_{SG}$ allows to asses on the spin-glass character of the compounds at low temperature [37], the frustration in the metal oxides is reflected by a value of $|\theta_W|/T_{SG} > 1$. The minimum along the series is found for R = Dy: $|\theta_W|/T_{SG} = 3.24$, thus all members of the series qualify as good spin-glasses after this criterion. As shown in Sections 3.2 and 3.3 the presence of a magnetic R modulates the temperature of the spin-glass transition, since it introduces an additional degree of freedom to the frustrated and disordered magnetic lattice. We analyze below the role of single ion anisotropy and concomitant anisotropic interaction in this temperature domain.

At low temperatures the R-Fe interaction adopts the form of an anisotropic Hamiltonian in an effective S* = 1/2 spin formulation, by projecting the Hamiltonian of Eq. (4) onto the effective spin wavefuncions $|S_z^*= \pm 1/2\rangle$ for the R atom. Such an anisotropic exchange Hamiltonian can be segregated into two parts, the isotropic Heisenberg, and the non-Heisenberg anisotropic component.

At temperatures much lower than the excitation energy to the first excited level E_1, the compounds containing a magnetic R may be classified as:

a) isotropic, R = Gd, Eu and Tm,
b) Kramers ions with uniaxial anisotropy, R = Dy and Er, planar anisotropy R = Sm, or weakly uniaxial, Yb,
c) non-Kramers ions with uniaxial anisotropy, Tb and Ho.

The ground state of the b) and c) classes is a doublet (Sm, Dy, Er), or a quasi-doublet (Tb, Ho) that can be described in terms of an effective S* = 1/2 spin. The relations $g_\alpha S_\alpha^* = g_J J_\alpha$ between the effective spin and total angular moment [38], allow to formulate the anisotropic Hamiltonian as

$$\mathscr{H}_{R,Fe}^{anis} = -2 \sum_{i>j}^{Fe,R} [J_{x,i,j}^* S_{x,i} S_{x,j}^* + J_{y,i,j}^* S_{y,i} S_{y,j}^* + J_{z,i,j}^* S_{z,i} S_{z,j}^*] \quad (9)$$

where the effective R-Fe interaction

$$J_{\alpha,i,j}^* = \tilde{J}_{i,j} \frac{g_\alpha}{g_J} \quad (10)$$

and α = x, y, z corresponding to the main directions of the g tensor describing the magnetic anisotropy of the ground doublet (or pseudo-doublet). The uniaxial ($g_x = g_y = 0$, $g_z \neq 0$), or planar ($g_x = g_y \neq 0$, $g_z = 0$) are the extreme cases of this Hamiltonian, which covers exactly, or approximately, all the magnetic R ions studied in this work. The isotropic Hamiltonian for Gd, is identical to that expressed in Eq. (4), with $g = 2$, while for Eu and Tm $g_\alpha = 0$ (see Table 3). Therefore, the R-Fe interactions in the spin glass may vary strongly as a function of the ground state single ion anisotropy.

Let us dwell on the qualitatively different result obtained for the interaction in the case of isotropic Gd^{3+} with respect to the anisotropic substitutions. We consider that in the $GdFeTi_2O_7$ compound the isotropic component is of paramount importance in R-Fe interaction, while in the R = Er, Dy, Ho and Tb substitutions, the R-Fe exchange is dominated by the uniaxial anisotropic component of the f-d exchange coupling. In the case of Sm, it has quasiplanar anisotropy. The effect of the magnetic interaction due to the presence of the magnetic R is to increase the T_{SG}. Let us analyze this statement.

$LuFeTi_2O_7$ which serves as *R* non-magnetic reference for the other compounds, has a spin-glass behavior due to the frustration and disorder of the Fe sublattice, and an average exchange interaction $J_{Fe,Fe}/k_B = -7.8$ K which gives rise to a transition temperature $T_{SG}^{Fe} = 5.2(5)$K. The compounds with a magnetic R modulates the exchange field acting on each Fe atom and produces an increase in the T_{SG} in the compound, $T_{SG}^R > T_{SG}^{Fe}$. The ratio $\Delta T_{SG}^R/T_{SG}^{Fe}$ is depicted in Fig. 9. Therefore, we ascribe the increase of the spin-glass temperature in $LuFeTi_2O_7$ when non-magnetic Lu^{3+} ion is replaced by another rare-earth, as due to increased magnetic correlations.

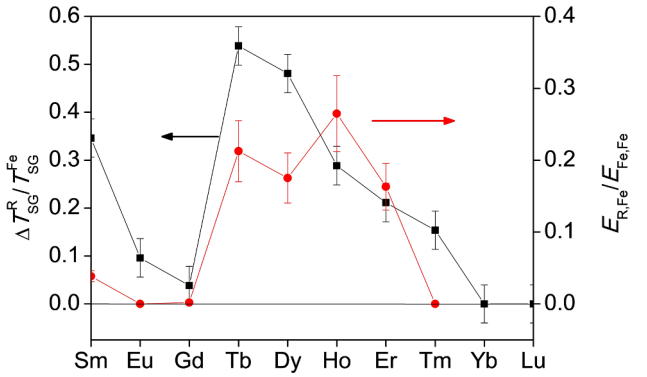

Fig. 9. Comparison of the R-dependence of Eq. (11) (red circles, right axis) with the relative variation of the spin glass transition temperature, $\Delta T_{SG}^R/T_{SG}^{Fe}$ (black squares, left axis). (For interpretation of the references to color in this figure legend, the reader is referred to the web version of this article.)

In particular, in the series of uniaxial anisotropic compounds, R = Tb, Dy, Ho and Er, the anisotropic exchange plays an important role in the dependence of ΔT_{SG}^R on the R substitution, as can be inferred from the linear dependence of $J_{\alpha,i,j}^*$ on g_z (Eq. (10)). Besides, since the T_{SG} in a spin-glass depends on the disorder geometry and frustration of the antiferromagnetically coupled spins in these compounds, we may assume along the series that the dependence on the geometry is identical in all cases, and the degree of frustration, as measured by the $|\theta_W|/T_{SG}$ ratio, is similar. Thus we may conjecture that T_{SG} has the same dependence on the average exchange $J_{i,j}$ interaction along the series, and consequently, ΔT_{SG}^R would be proportional to the increase in interaction energy. This proposition is formulated as:

$$\Delta T_{SG}^R/T_{SG}^{Fe} \sim \frac{E_{R,Fe}}{E_{Fe,Fe}} \quad (11)$$

where $E_{Fe,Fe} = N z_{Fe,Fe} |J_{Fe,Fe}| S^2$ is the average Fe-Fe interaction energy, and $E_{R,Fe} = N \bar{z}_{R,Fe} g_z |\tilde{J}_{R,Fe}| S_z S_z^*/g_J$ is the average low temperature R-Fe interaction energy in terms of the effective $S^* = 1/2$ model, for the compounds with uniaxial anisotropy. $\bar{z}_{R,Fe} = 3$ is the average nearest neighbor coordination number. In these compounds it has been considered that the isotropic interaction is negligible as compared to the anisotropic one.

For R = Sm the anisotropy is planar, in this case $E_{Sm,Fe} = N \bar{z}_{Sm,Fe} g_\perp |\tilde{J}_{R,Fe}| S_\perp S_\perp^*/g_J$ with $g_\perp = g_{x,y} \approx 0.47$. For R = Yb the anisotropy is weakly uniaxial, and has the largest crystal field ($E_1 = 463$ K). Using the expression for the uniaxial case, with $g_z = 5.41$ and $\tilde{J}_{Yb,Fe}/k_B = -6.51$ K (see Table 3), one obtains the ratio $E_{Yb,Fe}/E_{Fe,Fe} = 0.8$. This value is completely off from the experiment. The reason is that the method to determine the high temperature R-Fe interaction is not applicable with such a large crystal field splitting to the next excited electronic level.

In Fig. 9, we compare the experimental relative increase $\Delta T_{SG}^R/T_{SG}^{Fe}$ against the relation of Eq. (11), where the interaction constants for the different R have been taken from Table 3; i.e. from the high temperature determination

The agreement is satisfactory; indeed, the prediction of ΔT_{SG}^R for Gd has a negligible value, and for Tb, Dy, Ho and Er uniaxial anisotropic compounds, it is comparable to the experiment. Although the prediction is qualitatively correct, for Sm it falls short of the experimental value for $\Delta T_{SG}^R/T_{SG}^{Fe}$. It is the only case where the anisotropy is planar, so the model seems to work better for the uniaxial cases. The cases of the underestimation for Eu and Tm are different. The reason is that in our model we have not considered the magnetism coming from excited electronic states. The prediction for Yb is disregarded because one of the conditions for the model to be applicable is not fulfilled, namely that the asymptotic Curie Weiss law is obeyed in the 200–300 K

temperature region. Overall, the differences found are larger than the error bars, so probably, the model needed to describe better such R Fe spin glasses requires more details of the interactions and their pathways. For this purpose, Montecarlo simulations may be desirable, although such calculations fall beyond the scope of this work.

Previously, the important role of anisotropic non-Heisenberg exchange has been demonstrated in orthoferrites, where the isotropic part of the exchange interaction is almost completely compensated by the AF ordering of the d ions (Fe^{3+}) [36]. Spectroscopic measurements showing the increase in the rare-earth ground state exchange splitting for the magnetic configuration stable at low temperatures indicate a larger anisotropic contribution for the more anisotropic R^{3+} ions.

In mixed-valence Fe phosphate spin glasses, where Fe^{2+} ions have uniaxial anisotropy while Fe^{3+} are isotropic, the increase in the fraction of Fe^{2+} has the effect of increasing the freezing temperature, since anisotropy tends to suppress fluctuations [8].

In previous studies on these $RFeTi_2O_7$ compounds it had been argued that the spin glass state was associated to frustration caused by the competitive magnetic interactions between Fe^{3+} ions in different crystallographic sites and the occupational disorder, independently of the nature of the rare-earth ion [20,25]. This holds true in this series with substituted magnetic R. Similarly to the case of the Fe Phosphate glasses [8], the inclusion of the uniaxial anisotropic R ions has the effect of increasing T_{SG} by reducing the spin fluctuations, since the magnetic barrier to be overcome in a fluctuation is enhanced in the anisotropic case. Usually in spin glass systems, a higher degree of frustration reduces ordering temperature through frustration driven fluctuations. We observe that anisotropy is partially quenching the effect of frustration, suppressing fluctuations and increasing the freezing temperature.

5. Conclusions

Polycrystalline $RFeTi_2O_7$ (R = Eu, Gd, Dy, Ho, and Er) were produced by ceramic sintering at 1250 K and have been investigated using X-ray powder diffraction, and further characterized by specific heat, magnetization and frequency dependent ac susceptibility measurements.

The X-ray measurement indicates that $RFeTi_2O_7$ is orthorhombic, space group *Pcnb* at 300 K. The specific features of the structural characterization include the availability of the different non-equivalent positions for the magnetic Fe^{3+} ions in the unit cell of this material. A random site occupancy of the mixed octahedral sites (Ti/Fe) in all compounds, indicating a disorder of the magnetic iron ions distribution was observed. The disorder and the competing magnetic interactions in insulating $RFeTi_2O_7$ system leads to the formation of spin glass magnetic state at low temperatures. All the studied $RFeTi_2O_7$ compounds, with predominantly antiferromagnetic coupling, undergo a spin glass transition at a temperature T_{SG} which varies with the rare-earth ion.

The results of the temperature dependence of the heat capacity measurements show that no anomalies are observed in the temperature range of 2.0–100 K. So there are no long range ordering transitions in $RFeTi_2O_7$ compound. The transition to as spin-glass state is manifested with a very broad contribution centred at 5–10 K.

The thorough comparison of the spin glass properties of both, the series for R = Eu, Gd, Dy, Ho and Er, together with previous results for Tb and Lu, Tm and Yb, has drawn a picture of the active role played by rare earth in insulated spin glasses containing a 3d metal, Fe^{3+} and a 4f rare earth ion, R^{3+}. Magnetic rare earth ions participate in the spin glass transition through the interaction with the Fe^{3+} lattice.

The observed effects of the R substitution in the comparable uniaxial anisotropic compounds R = Er, Ho, Dy and Tb, are an increasing coercive field and increasing T_{SG}, in that trend. Also with that trend we find a slowing down of the characteristic spin relaxation time to values typical of cluster glass. That is, the substitution of non-magnetic Lu by high anisotropic rare earth ions, favours the formation of clusters with slower spin relaxation times.

Within an effective spin model, valid in the low temperature range where the spin-glass characteristics show up, such as transition temperature T_{SG}, and rounded heat capacity (approx. 1–10 K), it has been shown that the single ion ground state anisotropy reduces fluctuations and gives rise to an increase in T_{SG}. The relative increase in the spin-glass temperature $\Delta T_{SG}^{R}/T_{SG}^{Fe}$ with respect to the $LuFeTi_2O_7$, where Lu is non-magnetic, correlates qualitatively with the product of the ratio g_z/g_J (R = Tb, Dy, Ho, and Er), or $g_\perp/g_J$ (R = Sm) times the ratio of exchange interactions $\tilde{J}_{R,Fe}/J_{Fe,Fe}$, determined from the paramagnetic room temperature susceptibility measurements.

This work provides original relevant information of the interplay of interactions in insulating spin glasses containing both, rare-earth and transition metal ions, where the presence of anisotropic R modulated their spin-glass characteristics.

CRediT authorship contribution statement

A. Arauzo: Methodology, Investigation, Formal analysis, Writing - review & editing. **J. Bartolomé:** Conceptualization, Investigation, Formal analysis. **J. Luzón:** Formal analysis. **T. Drokina:** Conceptualization, Resources. **G.A. Petrakovskii:** Conceptualization, Supervision. **M.S. Molokeev:** Investigation, Formal analysis.

Declaration of Competing Interest

The authors declare that they have no known competing financial interests or personal relationships that could have appeared to influence the work reported in this paper.

Acknowledgements

This study has been financed by MECOM Project MAT2014-53921-R, MICINN Project MAT2017-83468-R and Gobierno de Aragón RASMIA E12_17R. Authors would like to acknowledge the use of Servicio General de Apoyo a la Investigación-SAI, Universidad de Zaragoza.

Appendix A. Supplementary data

Supplementary data to this article can be found online at https://doi.org/10.1016/j.jmmm.2020.167273.

References

[1] I.Y. Korenblit, E.F. Shender, Sov. Phys. - Uspekhi 32 (1989) 139–162.
[2] J.A. Mydosh, Spin-Glasses: An Experimental Introduction, Taylor&Fra, 1993.
[3] J.A. Mydosh, Reports, Prog. Phys. 78 (2015) 52501.
[4] G.A. Petrakovskii, K.S. Aleksandrov, L.N. Bezmaternikh, S.S. Aplesnin, B. Roessli, F. Semadeni, A. Amato, C. Baines, J. Bartolomé, M. Evangelisti, Phys. Rev. B 63 (2001) 184425.
[5] H. Kawamura, T. Taniguchi, Handb. Magn. Mater. 24 (2015) 1–137.
[6] H. Akamatsu, J. Kawabata, K. Fujita, S. Murai, K. Tanaka, Phys. Rev. B 84 (2011) 144408/1–8.
[7] H. Akamatsu, K. Fujita, S. Murai, K. Tanaka, Phys. Rev. B 81 (2010) 014423/1–9.
[8] H. Akamatsu, S. Oku, K. Fujita, S. Murai, K. Tanaka, Phys. Rev. B - Condens. Matter Mater. Phys. 80 (2009).
[9] V.V. Eremenko, V.A. Sirenko, A. Baran, E. Čižmár, A. Feher, J. Phys. Condens. Matter 30 (2018) 205801.
[10] R. Mathieu, A. Asamitsu, Y. Kaneko, J.P. He, Y. Tokura, Phys. Rev. B 72 (2005) 014436.
[11] M.B. Salamon, M. Jaime, Rev. Mod. Phys. 73 (2001) 583–628.
[12] M.-H. Phan, T.-L. Phan, T.-N. Huynh, S.-C. Yu, J.R. Rhee, N. Van Khiem, N.X. Phuc, J. Appl. Phys. 95 (2004) 7531–7533.
[13] N. Hasselmann, A.H. Castro Neto, C. Morais Smith, Phys. Rev. B 69 (2004) 014424.
[14] A. Malinowski, V.L. Bezusyy, R. Minikayev, P. Dziawa, Y. Syryanyy, M. Sawicki, Phys. Rev. B 84 (2011) 024409/1–17.
[15] A. Arauzo, N.V. Kazak, N.B. Ivanova, M.S. Platunov, Y.V. Knyazev, O.A. Bayukov, L.N. Bezmaternykh, I.S. Lyubutin, K.V. Frolov, S.G. Ovchinnikov, J. Bartolomé, J. Magn. Magn. Mater. 392 (2015) 114–125.
[16] H. Maletta, G. Aeppli, S.M. Shapiro, J. Magn. Magn. Mater. 31–34 (1983) 1367–1372.
[17] R. Mathieu, Y. Tokura, J. Phys. Soc. Japan 76 (2007) 124706.

[18] Y. Okimoto, H. Matsuzaki, Y. Tomioka, I. Kezsmarki, T. Ogasawara, M. Matsubara, H. Okamoto, Y. Tokura, J. Phys. Soc. Japan 76 (2007) 043702.
[19] C.S. Hong, W.S. Kim, E.O. Chi, N.H. Hur, Y.N. Choi, Chem. Mater. 14 (2002) 1832–1838.
[20] T.V. Drokina, G.A. Petrakovskii, M.S. Molokeev, A. Arauzo, J. Bartolomé, Phys. Procedia (2015) 580–588.
[21] T.V. Drokina, G.A. Petrakovskii, D.A. Velikanov, M.S. Molokeev, Solid State Phenom. 215 (2014) 470–473.
[22] T.V. Drokina, G.A. Petrakovskii, M.S. Molokeev, D.A. Velikanov, O.N. Pletnev, O.A. Bayukov, Phys. Solid State 55 (2013) 2037–2042.
[23] G.A. Petrakovskii, T.V. Drokina, A.L. Shadrina, D.A. Velikanov, O.A. Bayukov, M.S. Molokeev, A.V. Kartashev, G.N. Stepanov, Phys. Solid State 53 (2011) 1855–1858.
[24] T.V. Drokina, G.A. Petrakovskii, M.S. Molokeev, D.A. Velikanov, Phys. Solid State 60 (2018) 532–536.
[25] T.V. Drokina, G.A. Petrakovskii, O.A. Bayukov, M.S. Molokeev, J. Bartolomé, A. Arauzo, J. Magn. Magn. Mater. 440 (2017) 41–43.
[26] G.A. Petrakovskii, T.V. Drokina, D.A. Velikanov, O.A. Bayukov, M.S. Molokeev, A.V. Kartashev, A.L. Shadrina, A.A. Mitsuk, Phys. Solid State 54 (2012) 1813–1816.
[27] E.A. Genkina, V.I. Andrianov, E.L. Belokoneva, B.V. Mill, B.A. Maksimov, R.A. Tamazyan, Sov. Phys. Crystallogr 36 (1991) 796–800.
[28] B.O. Roos, P.A. Malmqvist, Phys. Chem. Chem. Phys. 6 (2004) 2919.
[29] F. Aquilante, J. Autschbach, R.K. Carlson, L.F. Chibotaru, M.G. Delcey, L. De Vico, I. Fdez, N. Galván, L.M. Ferré, L. Frutos, M. Gagliardi, A. Garavelli, C.E. Giussani, G. Li Hoyer, H. Manni, D. Lischka, P.Å. Ma, T. Malmqvist, A. Müller, M. Nenov, T.B. Olivucci, D. Pedersen, F. Peng, B. Plasser, M. Pritchard, I. Reiher, I. Rivalta, J. Schapiro, M. Segarra-Martí, D.G. Stenrup, L. Truhlar, A. Ungur, S. Valentini, V. Vancoillie, V.P. Veryazov, O. Vysotskiy, F. Weingart, R. Lindh Zapata, J. Comput. Chem. 37 (2016) 506–541.
[30] B.O. Roos, R. Lindh, P.Å. Malmqvist, V. Veryazov, P.O. Widmark, Chem. Phys. Lett. 409 (2005) 295–299.
[31] M. Andruh, P. Porchers, Inorg. Chem. 32 (1993) 1616–1622.
[32] D.N.H. Nam, R. Mathieu, P. Nordblad, N.V. Khiem, N.X. Phuc, Phys. Rev. B 62 (2000) 8989–8995.
[33] K. Vijayanandhini, C. Simon, V. Pralong, V. Caignaert, B. Raveau, Phys. Rev. B 79 (2009) 22440/1–10.
[34] S. Pakhira, C. Mazumdar, R. Ranganathan, S. Giri, M. Avdeev, Phys. Rev. B 94 (2016) 104414/1–15.
[35] P. Bag, P.R. Baral, R. Nath, Phys. Rev. B 98 (2018) 144436.
[36] K.P. Belov, A.K. Zvezdin, A.M. Kadomtseva, in:, I.M. Khalatnikov (Ed.), Phys. Rev., 1987, pp. 117–222.
[37] A.P. Ramirez, Annu. Rev. Mater. Sci. 24 (1994) 453–480.
[38] A. Abragam, B. Bleaney, in: Electron Paramagn. Reson. Transit. Ions, Clarendon Press - Oxford, 1970, p. Chapter 10.